Journal Pre-proofs

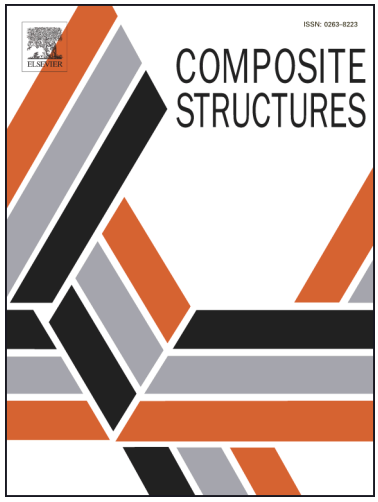

Predicting Global Strain Limits for Corrugated Panels

C. Wang, Y. Xia, M.I. Friswell, E.I. Saavedra Flores

PII: S0263-8223(19)32866-1
DOI: https://doi.org/10.1016/j.compstruct.2019.111472
Reference: COST 111472

To appear in: *Composite Structures*

Received Date: 30 July 2019
Accepted Date: 17 September 2019

Please cite this article as: Wang, C., Xia, Y., Friswell, M.I., Flores, E.I.S., Predicting Global Strain Limits for Corrugated Panels, *Composite Structures* (2019), doi: https://doi.org/10.1016/j.compstruct.2019.111472

Predicting Global Strain Limits for Corrugated Panels

C. Wang[a], Y. Xia[a,1], M.I. Friswell[a], E.I. Saavedra Flores[b]

[a] *College of Engineering, Swansea University, Swansea SA2 8PP, UK*
[b] *Departamento de Ingeniería en Obras Civiles, Universidad de Santiago de Chile. Av. Ecuador 3659, Santiago, Chile.*

Abstract

Corrugated panels have many potential applications in civil, mechanical and aerospace engineering. The research on morphing aircraft requires the derivation of deformation limits of corrugated panels, which can be used as the constraint conditions for the design and optimisation of morphing structures. The relationship between the local and global strains of the equivalent models for corrugated panels is derived, which makes the prediction of the maximum strain available. Thus, from the maximum strain criterion, the global strain limit is evaluated under different load conditions. The results from the proposed analytical method are compared to those from detailed finite element models, which indicates a good agreement for all of the analysed cases. The influence of the geometric parameters of the corrugation shape is also investigated.

Keywords: Corrugated panel, equivalent orthotropic plate, equivalent model, strain limit, morphing skin

1. Introduction

Corrugated structures are widely used in civil, aerospace and marine engineering, such as the applications in transportation vehicles, building roofs, steal bridges, corrugated walls, etc. There have been a lot of research work focused on the mechanical behaviour of the sandwiched structures with cor-

[1]Corresponding author. Tel: + 44 (0) 1792 295514.
Email address: yuying.xia@swansea.ac.uk

rugated cores using Finite Element (FE) [1–6], analytical [1, 2, 4, 6, 7] and experimental methods [2, 6, 7]. Based on the analytical models, optimisation designs of the sandwich structures with corrugated cores are performed when they are subject to static compression and blast loads [8, 9].

Morphing aircraft have drawn much attention in the last few years since they have the potential to improve aircraft performance [10–13]. One of the difficulties of realising a promising morphing aircraft is the morphing skin, which should allow the shape-changing and transfer local loads to the inner structure [14, 15] simultaneously. The corrugated panel has potential as a candidate morphing skin since its mechanical properties are inherently anisotropic, and the stiffness can be tailored by changing the corrugation shape [16–18].

To reduce the computational time, corrugated panels can be treated as orthotropic plates and the equivalent stiffness can be obtained by analytical or FE methods. For isotropic materials, Briassoulis [19] investigated the flexural stiffness and McFarland [20] investigated the shear stiffness. Samanta and Mukhopadhyay [21] focused on the static and dynamic analyses of trapezoidal corrugated panels by considering both extensional and flexural rigidities. Yokozeki et al. [16] investigated the properties of corrugated laminates made from carbon epoxy composites by experimental and analytical methods. Thill et al. [18, 22] compared the homogenized plate properties to the experimental results, and applied the corrugated panel in the morphing trailing edge [17]. Kress and Winkler [23] derived the analytical expressions of the equivalent orthotropic plate when the corrugations are defined as circular arcs. A planar finite element was developed [24], and the transverse shear response was also taken into account by Filipovic and Kress [25, 26]. Dayyani et al. [27] investigated the tensile and flexural properties of corrugated laminate panels using numerical and experimental methods. Bartolozzi et al. [28] investigated sinusoidal corrugated panels by the analytical and numerical methods, and the acoustic performance was also considered. Ye et al.

[29] adopted the variational asymptotic method to establish the equivalent model based on classical plate theory. Castigliano's theorem was used by Mohammadi et al. [30] to determine the analytical formulations of trapezoidal corrugated panels, and the analytical results were validated by tensile tests. Axial and bending coupling was found when one end of the corrugated panel was fixed, and the influence of the coupling on a morphing structure was discussed by Wang et al. [31]. Nonlinear properties were also investigated by Bai et al. [32] on the tensile properties of corrugated panels using a semi-analytical method. Kress and Filipovic recently proposed a nonlinear analytical model to investigate the circular corrugated panels with high amplitudes [33] and the manufacturing methods for the high-amplitude corrugated panels were investigated using numerical simulation and experimental demonstration [34].

In addition to the equivalent stiffnesses, morphing aircraft research also demands deformation limits to be used as design constraints, especially for the conceptual study of morphing aircraft. The deformation limit is the maximum deformation that the morphing structure can undergo, and the morphing structure will fail when the deformation is beyond this limit. Obviously, the deformation of the corrugated panel is determined by the structural layout and the load case, and the local deformation is varied in different areas of the corrugation due to the geometry. Thus, an analytical model, which can predict the global deformation limit of a corrugated panel is very useful in the design of morphing aircraft. However, compared to the research on the equivalent stiffness of corrugated panels, there are few papers considering the deformation limits of corrugated panels. Winkler and Kress [35] investigated the deformation limits for corrugated laminates, although the analysis was only applied to circular corrugations. Schmitz and Horst [36] investigated the bending deformation limit of circular corrugated panels, which were manufactured from unidirectionally reinforced composites and tested to verify the predicted curvature limits.

To perform the optimisation of morphing aircraft, a general model of the corrugated panel, which can predict both the equivalent stiffnesses and the deformation limits under different load cases for different corrugation shapes and materials, is expected. Xia et al. [37] proposed an equivalent model to predict the equivalent stiffness of the corrugated panel. The current research will further extend this model with the capability to predict the deformation limit. Section 2 will give a brief review of the proposed equivalent model. Then, in Section 3, the relationship between the local and global strains is deduced. Numerical validation of the relationships between the global and local strains are then performed for both trapezoidal and round corrugations using detailed finite element analysis. The deformation limit of the corrugated panel can then be predicted using a maximum strain criterion. Section 4 demonstrates the process to obtain the strain limit of the corrugated panel made from the single layer panel. The influence of geometric parameters is also investigated in Section 5.

2. Equivalent Stiffness Properties for Corrugated Panels

2.1. Equivalent Orthotropic Plate Model

The corrugated panels are generated from a periodic shape in the xz plane that is extruded in the y direction to produce a panel. The geometry of a corrugation unit is shown in Figure 1. There are two coordinate systems that must be defined to analyse the panel, namely the global xyz Cartesian coordinate system as shown in Figure 1, and the local coordinate system on the sheet forming the corrugation. The local coordinate system is defined by the tangent direction to the sheet in the xz plane, defined as the s direction, and the normal to the sheet in the xz plane, defined as the n direction. Both of these directions are shown in Figure 1. For convenience, and without loss of generality, it is assumed that the principal directions of the orthotropic sheet forming the corrugations coincide with the coordinates y and s of the plate.

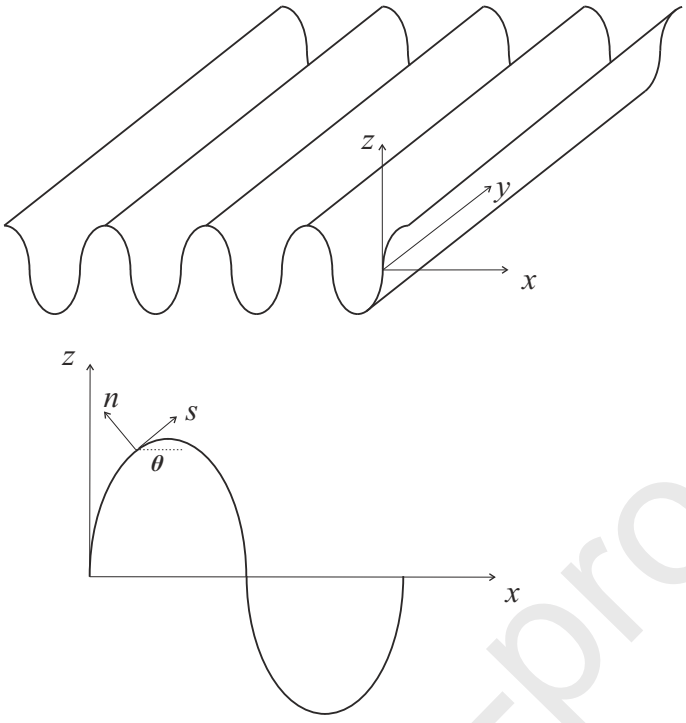

Figure 1: Definition of the coordinate systems.

The corrugated panel is approximated by an orthotropic classical Kirchhoff plate, by ignoring the coupling stiffness matrix. The constitutive equation of the equivalent orthotropic plate is

$$\begin{Bmatrix} \bar{N}_x \\ \bar{N}_y \\ \bar{N}_{xy} \\ \bar{M}_x \\ \bar{M}_y \\ \bar{M}_{xy} \end{Bmatrix} = \begin{bmatrix} \bar{A}_{11} & \bar{A}_{12} & 0 & 0 & 0 & 0 \\ \bar{A}_{12} & \bar{A}_{22} & 0 & 0 & 0 & 0 \\ 0 & 0 & \bar{A}_{66} & 0 & 0 & 0 \\ 0 & 0 & 0 & \bar{D}_{11} & \bar{D}_{12} & 0 \\ 0 & 0 & 0 & \bar{D}_{12} & \bar{D}_{22} & 0 \\ 0 & 0 & 0 & 0 & 0 & \bar{D}_{66} \end{bmatrix} \begin{Bmatrix} \bar{\epsilon}_x \\ \bar{\epsilon}_y \\ \bar{\gamma}_{xy} \\ \bar{\kappa}_x \\ \bar{\kappa}_y \\ \bar{\kappa}_{xy} \end{Bmatrix} \tag{1}$$

where $\bar{\epsilon}_x, \bar{\epsilon}_y, \bar{\gamma}_{xy}, \bar{\kappa}_x, \bar{\kappa}_y, \bar{\kappa}_{xy}$ denote the strain components and curvature components of the mid-plane of the orthotropic plate model, and $\bar{N}_x$, $\bar{N}_y$, $\bar{N}_{xy}$, $\bar{M}_x$, $\bar{M}_y$, $\bar{M}_{xy}$ denote the force and moment components.

2.2. Stiffness Properties for Corrugated Panels

The equivalent stiffness properties for corrugated panels were derived by Xia et al. [37]. Table 1 summarises the stiffness terms for a general corrugation defined by $(x(s), z(s))$. The constants that must be calculated for a given corrugation geometry are the half period c, the corrugation half length l, and the integrals I_1 and I_2.

3. Relationship between global and local strains

3.1. Local strain expressions under single global deformation type

In the local curvilinear coordinates (s, n, y), we have,

$$\begin{Bmatrix} N_s \\ N_y \\ N_{sy} \\ M_s \\ M_y \\ M_{sy} \end{Bmatrix} = \begin{bmatrix} A_{11} & A_{12} & 0 & 0 & 0 & 0 \\ A_{12} & A_{22} & 0 & 0 & 0 & 0 \\ 0 & 0 & A_{66} & 0 & 0 & 0 \\ 0 & 0 & 0 & D_{11} & D_{12} & 0 \\ 0 & 0 & 0 & D_{12} & D_{22} & 0 \\ 0 & 0 & 0 & 0 & 0 & D_{66} \end{bmatrix} \begin{Bmatrix} \epsilon_s \\ \epsilon_y \\ \gamma_{sy} \\ \kappa_s \\ \kappa_y \\ \kappa_{sy} \end{Bmatrix} \tag{2}$$

where ϵ_s, ϵ_y, γ_{sy}, κ_s, κ_y, and κ_{sy} denote the strain components and curvature components of the mid-plane of the orignial sheet in the local curvilinear coordinates. Suppose that the global strain components and curvature components, $\bar{\epsilon}_x$, $\bar{\epsilon}_y$, $\bar{\gamma}_{xy}$, $\bar{\kappa}_x$, $\bar{\kappa}_y$, $\bar{\kappa}_{xy}$, of the mid-plane of the equivalent orthotropic plate model are independent. The local strain will be derived under the six global strain boundary conditions as follows.

3.1.1. Case 1: $\left[\bar{\boldsymbol{\epsilon}}^T, \bar{\boldsymbol{\kappa}}^T\right] = [\bar{\epsilon}_x, 0, 0, 0, 0, 0]$

The symmetry of the corrugations and the boundary conditions require that most of the local strains are zero; thus $\epsilon_y = 0$, $\gamma_{sy} = 0$, $\kappa_y = 0$ and $\kappa_{sy} = 0$. Since the only strain is in the x direction, the internal force in the x direction for the corrugated sheet must be constant, and hence the equilibrium of internal forces in the local coordinate system implies that

$$N_s = \bar{N}_x \frac{\mathrm{d}x}{\mathrm{d}s} = \bar{A}_{11} \bar{\epsilon}_x \frac{\mathrm{d}x}{\mathrm{d}s} \tag{3}$$

Table 1: Stiffness properties for a general corrugation, with half period c and half length l.

Stiffness Term	Expression (Xia et al. [37])
$\bar{A}_{11}$	$\dfrac{2c}{\left[\dfrac{I_1}{A_{11}}+\dfrac{I_2}{D_{11}}\right]}$
$\bar{A}_{12}$	$\dfrac{A_{12}}{A_{11}}\bar{A}_{11}$
$\bar{A}_{22}$	$\dfrac{\bar{A}_{12}A_{12}}{A_{11}}+\dfrac{l}{c}\dfrac{A_{11}A_{22}-A_{12}^2}{A_{11}}$
$\bar{A}_{66}$	$\dfrac{c}{l}A_{66}$
$\bar{D}_{11}$	$\dfrac{c}{l}D_{11}$
$\bar{D}_{12}$	$\dfrac{D_{12}}{D_{11}}\bar{D}_{11}$
$\bar{D}_{22}$	$\dfrac{1}{2c}\left[I_2A_{22}+I_1D_{22}\right]$
$\bar{D}_{66}$	$\dfrac{l}{c}D_{66}$

where for the trapezoidal corrugation:

$$I_1=\frac{4f\cos^2\alpha}{\sin\alpha}+2c-\frac{4f}{\tan\alpha}\quad\text{and}\quad I_2=\frac{4f^3}{3\sin\alpha}+2f^2(c-\frac{2f}{\tan\alpha})$$

for the round corrugation:

$$I_1=\pi R\quad\text{and}\quad I_2=\frac{4L^3}{3}+2\pi L^2R+8LR^2+\pi R^3$$

From Equation (2) and the zero strain in the y direction, we have

$$\epsilon_s = \frac{N_s}{A_{11}} = \frac{\bar{A}_{11}}{A_{11}} \frac{\mathrm{d}x}{\mathrm{d}s} \bar{\epsilon}_x \tag{4}$$

Comparing moments between the local and global coordinates systems gives

$$M_s = \bar{N}_x z = \bar{A}_{11} z \bar{\epsilon}_x \tag{5}$$

and zero local curvature $\kappa_y = 0$ gives

$$\kappa_s = \frac{M_s}{D_{11}} = \frac{\bar{A}_{11} z}{D_{11}} \bar{\epsilon}_x \tag{6}$$

3.1.2. Case 2: $\left[\bar{\boldsymbol{\epsilon}}^T, \bar{\boldsymbol{\kappa}}^T\right] = [0, \bar{\epsilon}_y, 0, 0, 0, 0]$

In this case, $\bar{N}_x = \bar{A}_{12}\bar{\epsilon}_y$ and $\bar{N}_y = \bar{A}_{22}\bar{\epsilon}_y$. The local strains are given by $\epsilon_y = \bar{\epsilon}_y$, $\gamma_{sy} = 0$, $\kappa_y = 0$ and $\kappa_{sy} = 0$. Equating forces in the local coordinate system gives

$$N_s = \bar{N}_x \frac{\mathrm{d}x}{\mathrm{d}s} = \bar{A}_{12} \frac{\mathrm{d}x}{\mathrm{d}s} \bar{\epsilon}_y \tag{7}$$

From Equation (2), $N_s = A_{11}\epsilon_s + A_{12}\epsilon_y$, and hence

$$\epsilon_s = \frac{N_s - A_{12}\epsilon_y}{A_{11}} = \frac{1}{A_{11}} \left(\bar{A}_{12} \frac{\mathrm{d}x}{\mathrm{d}s} - A_{12} \right) \bar{\epsilon}_y \tag{8}$$

Since

$$M_s = \bar{N}_x z = \bar{A}_{12} z \bar{\epsilon}_y \tag{9}$$

the zero local curvature, $\kappa_y = 0$, gives(from Equation (2))

$$\kappa_s = \frac{M_s}{D_{11}} = \frac{\bar{A}_{12} z}{D_{11}} \bar{\epsilon}_y \tag{10}$$

3.1.3. Case 3: $\left[\bar{\boldsymbol{\epsilon}}^T, \bar{\boldsymbol{\kappa}}^T\right] = [0, 0, \bar{\gamma}_{xy}, 0, 0, 0]$

In this case, we have $N_{sy} = \bar{N}_{xy} = \bar{A}_{66}\bar{\gamma}_{xy}$. The local strains are given by $\epsilon_s = 0$, $\epsilon_y = 0$, $\kappa_s = 0$, $\kappa_y = 0$ and $\kappa_{sy} = 0$. Obviously we have

$$\gamma_{sy} = \frac{N_{sy}}{A_{66}} = \frac{\bar{A}_{66}}{A_{66}} \bar{\gamma}_{xy} \tag{11}$$

3.1.4. Case 4: $\left[\bar{\boldsymbol{\epsilon}}^T, \bar{\boldsymbol{\kappa}}^T\right] = [0, 0, 0, \bar{\kappa}_x, 0, 0]$

In this case, $M_s = \bar{M}_x = \bar{D}_{11}\bar{\kappa}_x$. The local strains are given by $\epsilon_s = 0$, $\epsilon_y = 0$, $\gamma_{sy} = 0$, $\kappa_y = 0$ and $\kappa_{sy} = 0$. Thus,

$$\kappa_s = \frac{M_s}{D_{11}} = \frac{\bar{D}_{11}}{D_{11}} \bar{\kappa}_x \tag{12}$$

Table 2: Relationship between the global and local strains

	$\{\bar{\epsilon}_x, 0, 0, 0, 0, 0\}^T$	$\{0, \bar{\epsilon}_y, 0, 0, 0, 0\}^T$	$\{0, 0, \bar{\gamma}_{xy}, 0, 0, 0\}^T$
ε_s	$\frac{\bar{A}_{11}}{A_{11}}\frac{\mathrm{d}x}{\mathrm{d}s}\bar{\epsilon}_x$	$\frac{1}{A_{11}}\left(\bar{A}_{12}\frac{\mathrm{d}x}{\mathrm{d}s} - A_{12}\right)\bar{\epsilon}_y$	0
ε_y	0	$\bar{\epsilon}_y$	0
ε_{sy}	0	0	$\frac{\bar{A}_{66}}{A_{66}}\bar{\gamma}_{xy}$
κ_s	$\frac{\bar{A}_{11}z}{D_{11}}\bar{\epsilon}_x$	$\frac{\bar{A}_{12}z}{D_{11}}\bar{\epsilon}_y$	0
κ_y	0	0	0
κ_{sy}	0	0	0
	$\{0, 0, 0, \bar{\kappa}_x, 0, 0\}^T$	$\{0, 0, 0, 0, \bar{\kappa}_y, 0\}^T$	$\{0, 0, 0, 0, 0, \bar{\kappa}_{xy}\}^T$
ε_s	0	0	0
ε_y	0	$z\bar{\kappa}_y$	0
ε_{sy}	0	0	0
κ_s	$\frac{\bar{D}_{11}}{D_{11}}\bar{\kappa}_x$	0	0
κ_y	0	$\frac{\mathrm{d}x}{\mathrm{d}s}\bar{\kappa}_y$	0
κ_{sy}	0	0	$\bar{\kappa}_{xy}$

3.1.5. Case 5: $\left[\bar{\boldsymbol{\epsilon}}^T, \bar{\boldsymbol{\kappa}}^T\right] = [0, 0, 0, 0, \bar{\kappa}_y, 0]$

In this case, the local strains are given by $\epsilon_s = 0$, $\epsilon_y = z\bar{\kappa}_y$, $\gamma_{sy} = 0$, $\kappa_s = 0$, $\kappa_{sy} = 0$. Based on a simple geometry transformation, we have

$$\kappa_y = \frac{\mathrm{d}x}{\mathrm{d}s}\bar{\kappa}_y \tag{13}$$

3.1.6. Case 6: $\left[\bar{\boldsymbol{\epsilon}}^T, \bar{\boldsymbol{\kappa}}^T\right] = [0, 0, 0, 0, 0, \bar{\kappa}_{xy}]$

In this case, the local strains are $\epsilon_s = 0$, $\epsilon_y = 0$, $\gamma_{sy} = 0$, $\kappa_s = 0$, $\kappa_y = 0$. From the definition of $\bar{\kappa}_{xy}$, we have $\kappa_{sy} = \bar{\kappa}_{xy}$.

Table 2 summarizes the relationship between the global and local strains.

3.2. Local Strain Expression with Global Strain

As the global strain components $\bar{\epsilon}_x$, $\bar{\epsilon}_y$, $\bar{\gamma}_{xy}$, $\bar{\kappa}_x$, $\bar{\kappa}_y$, $\bar{\kappa}_{xy}$ are independent, the local strain under the boundary condition $\left[\bar{\boldsymbol{\epsilon}}^T, \bar{\boldsymbol{\kappa}}^T\right] = [\bar{\epsilon}_x, \bar{\epsilon}_y, \bar{\gamma}_{xy}, \bar{\kappa}_x, \bar{\kappa}_y, \bar{\kappa}_{xy}]$ can be obtained by the linear superposition of the six cases in Section 3.1. Thus, the local strain expression in matrix form is,

$$\begin{Bmatrix} \epsilon_s \\ \epsilon_y \\ \gamma_{sy} \\ \kappa_s \\ \kappa_y \\ \kappa_{sy} \end{Bmatrix} = \begin{bmatrix} T_{11} & T_{12} & 0 & 0 & 0 & 0 \\ 0 & T_{22} & 0 & 0 & T_{25} & 0 \\ 0 & 0 & T_{33} & 0 & 0 & 0 \\ T_{41} & T_{42} & 0 & T_{44} & 0 & 0 \\ 0 & 0 & 0 & 0 & T_{55} & 0 \\ 0 & 0 & 0 & 0 & 0 & T_{66} \end{bmatrix} \begin{Bmatrix} \bar{\epsilon}_x \\ \bar{\epsilon}_y \\ \bar{\gamma}_{xy} \\ \bar{\kappa}_x \\ \bar{\kappa}_y \\ \bar{\kappa}_{xy} \end{Bmatrix} \tag{14}$$

where

$$\begin{aligned} T_{11} &= \frac{\bar{A}_{11}}{A_{11}} \left(\frac{\mathrm{d}x}{\mathrm{d}s} \right) \\ T_{12} &= \frac{1}{A_{11}} \left(\bar{A}_{12} \frac{\mathrm{d}x}{\mathrm{d}s} - A_{12} \right) \\ T_{22} &= 1 \\ T_{25} &= z \\ T_{33} &= \frac{\bar{A}_{66}}{A_{66}} \\ T_{41} &= \frac{\bar{A}_{11} z}{D_{11}} \\ T_{42} &= \frac{\bar{A}_{12} z}{D_{11}} \\ T_{44} &= \frac{\bar{D}_{11}}{D_{11}} \\ T_{55} &= \frac{\mathrm{d}x}{\mathrm{d}s} \\ T_{66} &= 1 \end{aligned}$$

3.3. Numerical Validation

The proposed expressions are verified by two numerical examples, with trapezoidal and round corrugations, using the finite element method (FEM).

3.3.1. Trapezoidal corrugation

The first case is using the example taken from Xia et al. [37]. It has a trapezoidal corrugation shape shown in Figure 2a with an isotropic sheet material. The following properties for the trapezoidal corrugation profile are used

$$E = 210\,\text{GPa}, \quad \nu = 0.3, \quad b = 0.1\,\text{m}, \quad c = 0.0508\,\text{m},$$
$$f = 0.0127\,\text{m}, \quad t = 0.002\,\text{m}, \quad \alpha = 45^\circ.$$

where b is the width of the panel and t is the thickness of the sheet.

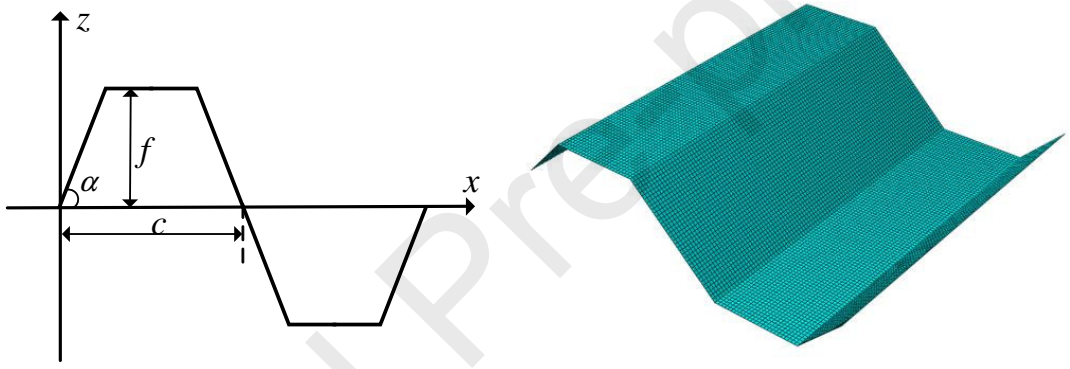

(a) (b)

Figure 2: (a) One period of a trapezoidal corrugation [37] (b) Detailed finite element model

A detailed finite element model (FEM) for one period of the trapezoidal corrugation was constructed using the commercial software Abaqus®. Figure 2b shows the mesh of this model, which has 12423 nodes and 12200 S4R shell elements. The mesh size is 1mm in this model. The general-purpose shell element S4R, which can be used to simulate both thick and thin plates [38], is adopted. The six boundary conditions mentioned in Section 3.1 were applied to the finite element model. The boundary conditions were applied to the edges of the corrugated panels, in conjunction with the constraints of the corresponding degrees of freedom between the structural nodes on the edges to ensure the finite element model can represent a periodic unit of the

corrugated panel. Figure 3 compares the 10 coefficients in Equation (14) for the proposed method with those obtained from the FEM, which shows that the proposed method clearly predicts the local strains very accurately.

3.3.2. Round corrugation

The second case tests the round corrugated panel, which is made from composite material. Figure 4a shows the geometry definition of the round corrugated panel. The material properties [35] are: axial modulus E_{11} = 54GPa, transverse modulus E_{22} = 13.5 GPa, shear modulus G_{12} = 4.46 GPa, Poisson's ratio $\nu_{12} = 0.26$. The stack sequence is $[90/0/90/0/90]^\circ$. In the current study, 0° is defined as the direction of the s axis and 90° as the direction of the y axis. The geometry parameters of the round corrugation are R=L=3mm, and the width of the panel is b=15mm. Each layer of the composite is assumed to have a thickness of 0.125mm.

The detailed finite element model for one period of the round corrugation, shown in 4b, is also built in the commercial software Abaqus® [38]. The mesh size is 0.5mm. The six boundary conditions mentioned in Section 3.1 are applied to the finite element model respectively. The strain and curvature components in the middle plane of the corrugated panels are obtained for validation. The transformation coefficients in Equation (14) of the round corrugated panel are compared in Figure 5. The local s axis instead of global x axis is adopted as the horizontal axis for visualisation purposes.

The comparisons in Figure 5 indicate that the proposed method can predict the local strains with good accuracy and the maximum error of the coefficients is below 5%.

4. Global Strain Limits

4.1. Maximum Strain Criterion

To estimate the global strain limits, the maximum strain criterion [39] is used, based on the material strain limits. Assuming linear-elasticity, the local strains must fulfil the strength limits given by

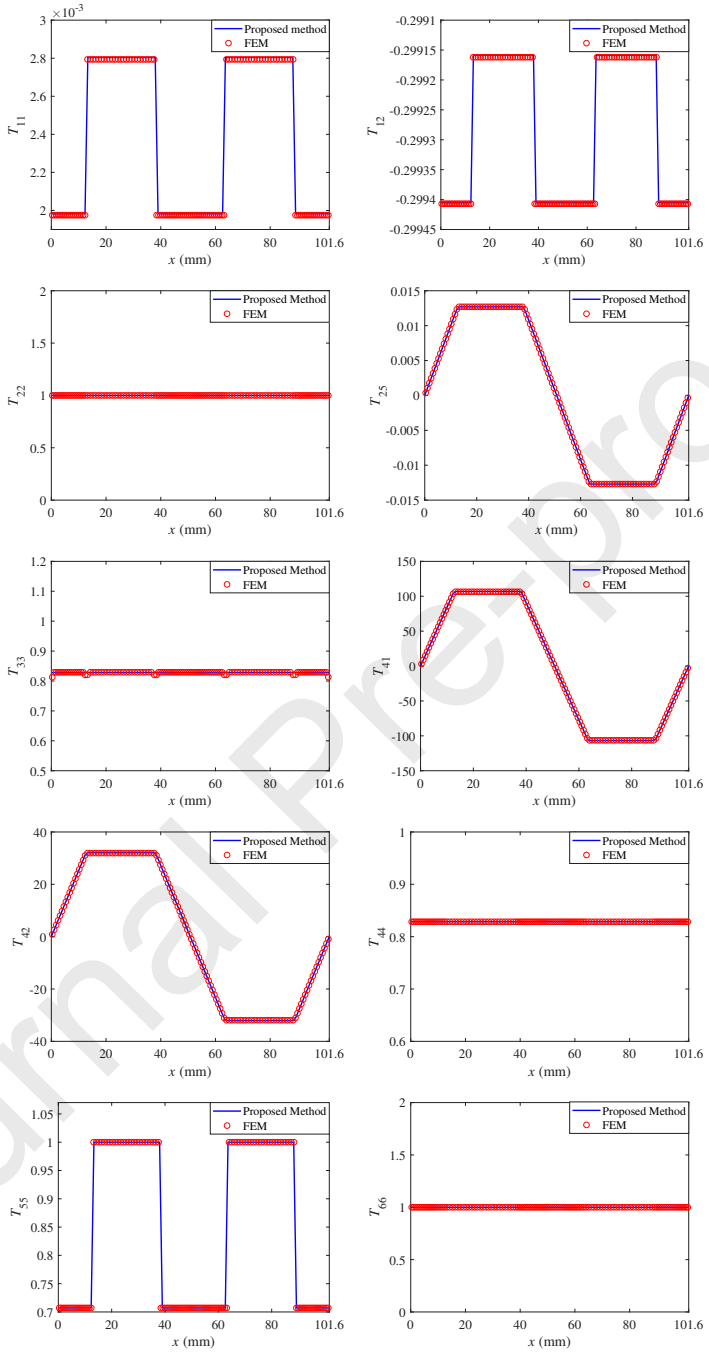

Figure 3: The transformation coefficients in Equation (14) for the trapezoidal corrugation predicted by the proposed method and by FEM

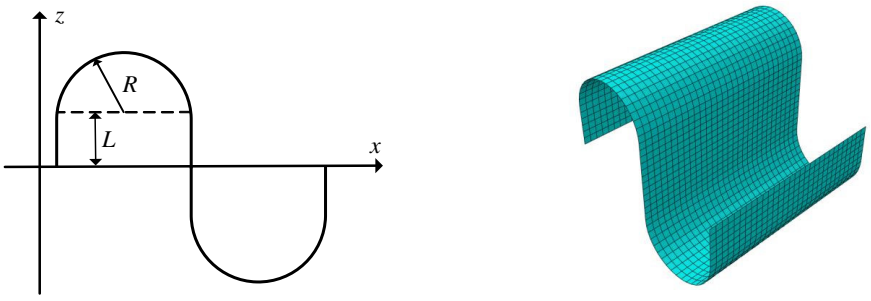

(a) (b)

Figure 4: (a) One period of a round corrugation [37] (b) Detailed finite element model

$$X_c/E_{11} \leq \epsilon_1 \leq X_t/E_{11}$$
$$Y_c/E_{22} \leq \epsilon_2 \leq Y_t/E_{22}$$
$$|\gamma_{12}| \leq S/G_{12}$$

Here, ϵ_1, ϵ_2 and $|\gamma_{12}|$ indicate the strain along the material axes. X_c, Y_c indicate the compressive strengths, X_t and Y_t represent the tensile strengths, and S indicates the shear strength. E_{11} and E_{22} are the Young's modulus along the material axes and G_{12} is the shear modulus.

4.2. Global strain limit of a single-layer panel

To estimate the global strain limit, we consider the six load cases mentioned in section 3.1. In the deductions below, we assume the lamina angle is 0°, which is along the s axis. For other lamina angles, the strain components in the principle axes can be further obtained using the classical composite theory, and then the maximum strain criterion can be adopted to obtain the global strain limit.

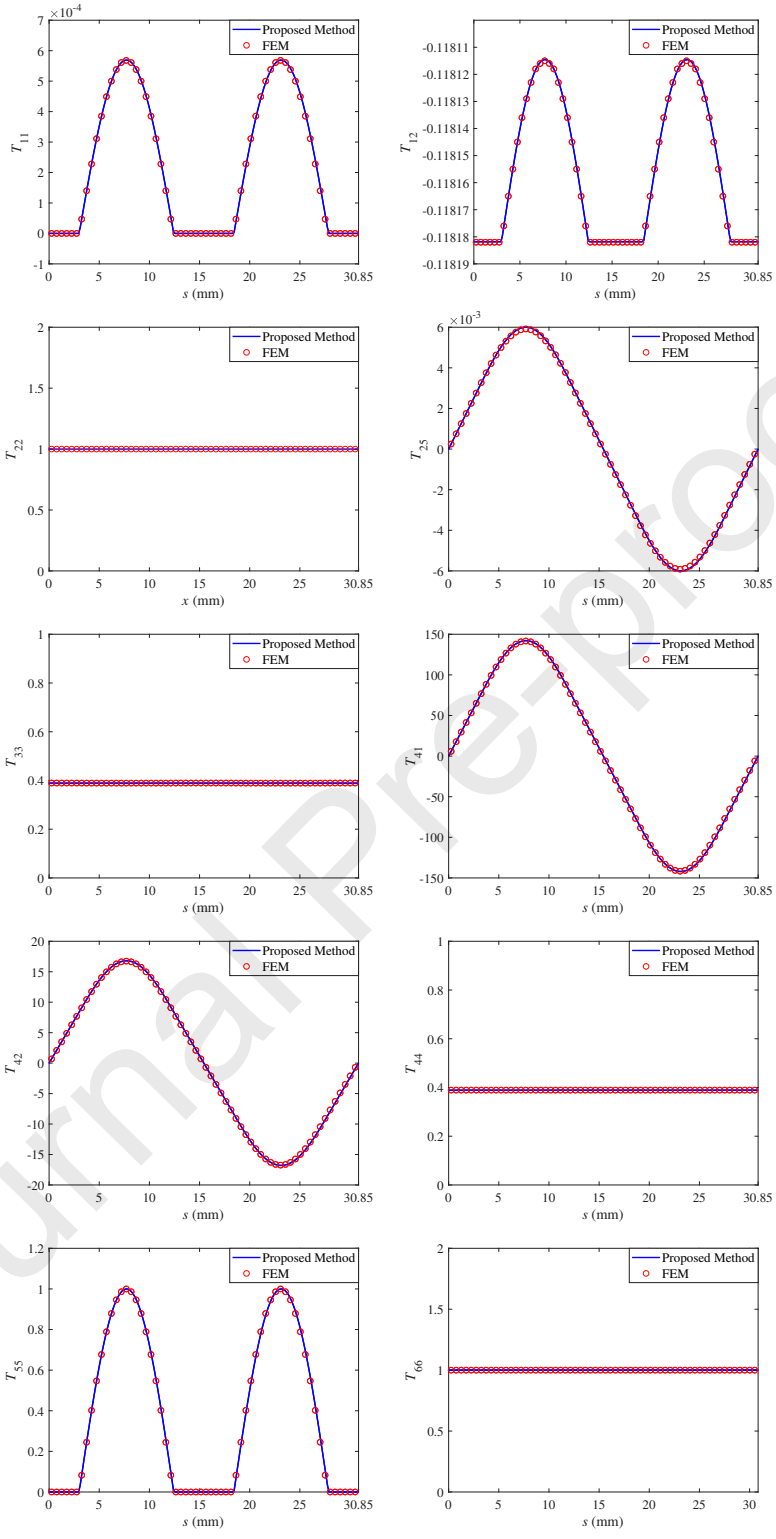

Figure 5: The transformation coefficients in Equation (14) for the round corrugation predicted by the proposed method and by FEM

4.2.1. Case 1: $\left[\bar{\boldsymbol{\epsilon}}^T, \bar{\boldsymbol{\kappa}}^T\right] = [\bar{\epsilon}_x, 0, 0, 0, 0, 0]$

From classical plate theory, at point (s, ξ), where ξ denotes the coordinate along the local thickness direction, the strain distribution is

$$\epsilon(s, \xi) = \epsilon_s + \xi\kappa_s = \left(\frac{\bar{A}_{11}}{A_{11}}\frac{dx}{ds} + \xi\frac{z\bar{A}_{11}}{D_{11}}\right)\bar{\epsilon}_x \tag{15}$$

Usually, the extreme value of local strain will occur at $z = \pm f$, where the extreme value of bending moment occurs. Here f denotes the height of the half-corrugation. At $z = \pm f$, for most corrugation shapes (except a triangle corrugation), $\mathrm{d}x/\mathrm{d}s = 1$. In this case, the extreme value of the local strain $\epsilon(s)$ is,

$$\hat{\epsilon}_s = \left(\frac{\bar{A}_{11}}{A_{11}} \pm \frac{\bar{A}_{11}ft}{2D_{11}}\right)\bar{\epsilon}_x \tag{16}$$

The global strain limits (both tension and compression limits) are then given by the following inequalities,

$$X_c/E_{11} \leq \left(\frac{\bar{A}_{11}}{A_{11}} + \frac{\bar{A}_{11}ft}{2D_{11}}\right)\bar{\epsilon}_x \leq X_t/E_{11}$$
$$X_c/E_{11} \leq \left(\frac{\bar{A}_{11}}{A_{11}} - \frac{\bar{A}_{11}ft}{2D_{11}}\right)\bar{\epsilon}_x \leq X_t/E_{11}$$

4.2.2. Case 2: $\left[\bar{\boldsymbol{\epsilon}}^T, \bar{\boldsymbol{\kappa}}^T\right] = [0, \bar{\epsilon}_y, 0, 0, 0, 0]$

In this case, the extreme value of the local strain $\epsilon(s)$ is,

$$\hat{\epsilon}_s = \left(\frac{\bar{A}_{12} - A_{12}}{A_{11}} \pm \frac{\bar{A}_{12}ft}{2D_{11}}\right)\bar{\epsilon}_y \tag{17}$$

Then we obtain the global strain limits by solving the following inequalities,

$$Y_c/E_{22} \leq \bar{\epsilon}_y \leq Y_t/E_{22}$$
$$X_c/E_{11} \leq \left(\frac{\bar{A}_{12} - A_{12}}{A_{11}} + \frac{\bar{A}_{12}ft}{2D_{11}}\right)\bar{\epsilon}_y \leq X_t/E_{11}$$
$$X_c/E_{11} \leq \left(\frac{\bar{A}_{12} - A_{12}}{A_{11}} - \frac{\bar{A}_{12}ft}{2D_{11}}\right)\bar{\epsilon}_y \leq X_t/E_{11}$$

4.2.3. Case 3: $\left[\bar{\boldsymbol{\epsilon}}^T, \bar{\boldsymbol{\kappa}}^T\right] = [0, 0, \bar{\gamma}_{xy}, 0, 0, 0]$

In this case,

$$|\gamma_{sy}| = \frac{\bar{A}_{66}}{A_{66}} |\bar{\gamma}_{xy}| \leq \frac{S}{G_{12}} \tag{18}$$

and hence,

$$|\bar{\gamma}_{xy}| \leq \frac{A_{66} S}{\bar{A}_{66} G_{12}} \tag{19}$$

4.2.4. Case 4: $\left[\bar{\boldsymbol{\epsilon}}^T, \bar{\boldsymbol{\kappa}}^T\right] = [0, 0, 0, \bar{\kappa}_x, 0, 0]$

In this case, the extreme value of the local strain is,

$$\hat{\epsilon}_s = \pm \frac{t}{2} \kappa_s = \pm \frac{\bar{D}_{11} t}{2 D_{11}} \bar{\kappa}_x \tag{20}$$

Then the global strain limit is obtained as,

$$|\bar{\kappa}_x| \leq \frac{2 D_{11}}{\bar{D}_{11} t} \min \left\{ X_t / E_{11}, -X_c / E_{11} \right\} \tag{21}$$

4.2.5. Case 5: $\left[\bar{\boldsymbol{\epsilon}}^T, \bar{\boldsymbol{\kappa}}^T\right] = [0, 0, 0, 0, \bar{\kappa}_y, 0]$

In this case, the extreme value of the local strain is,

$$\hat{\epsilon}_y = \pm \left(f + \frac{t}{2} \right) \bar{\kappa}_y \tag{22}$$

Then the global strain limits are obtained as follows,

$$|\bar{\kappa}_y| \leq \frac{1}{f + \frac{t}{2}} \min \left\{ Y_t / E_{22}, -Y_c / E_{22} \right\} \tag{23}$$

4.2.6. Case 6: $\left[\bar{\boldsymbol{\epsilon}}^T, \bar{\boldsymbol{\kappa}}^T\right] = [0, 0, 0, 0, 0, \bar{\kappa}_{xy}]$

In this case, the local strains are $\epsilon_s = 0$, $\epsilon_y = 0$, $\gamma_{sy} = 0$, $\kappa_s = 0$, $\kappa_y = 0$. Since the definition of $\bar{\kappa}_{xy}$ implies that $\kappa_{sy} = \bar{\kappa}_{xy}$,

$$\left| \frac{t}{2} \kappa_{sy} \right| \leq \frac{S}{G_{12}} \tag{24}$$

and then

$$|\bar{\kappa}_{xy}| \leq \frac{2S}{G_{12} t} \tag{25}$$

4.3. Global strain limits of a multi-layer composite laminate

The transformation equation has given the relationship between the global strain and the local strain components. The local strain components in Equation (14) are the strains in the middle plane of the corrugated panel. For a multi-layer composite laminate, the strain components of each layer can be further obtained from strain components of the middle plane in Equation (14) using the classical composite theory, then the maximum strain criterion can be adopted to give the global strain limit.

5. Case Study and Parametric Analysis

5.1. Trapezoidal corrugation

In this section, a trapezoidal corrugated panel made of isotropic material is investigated. The material properties are taken from Section 3.3.1, and the following strength limits are assumed: tensile strength is 350MPa, compressive strength is 144MPa, and the shear strength is 210MPa.

Table 3 gives the global strain limits. Figure 6 shows the variation of the normalised strain limits with the corrugation amplitude f. The normalised strain limit is defined as the ratio between the global strain limit of the corrugated panel and the flat panel.

5.2. Round corrugation

Round corrugated panels made of a single-layer composite and a multi-layer composite are studied in this section. The geometry of the corrugation and the composite material properties in Section 3.3.2 are used. The thickness of the single-layer composite panel is $t = 0.6$mm, and the lamina ply angle is $0°$. The multi-layer composite panel has the stack sequence $[90/45/0/\text{-}45/90]°$, and the thickness of each layer is 0.125mm. The following strength limits are assumed: $X_t = 1780$ MPa, $X_c = -700$ MPa, $Y_t = 65$ MPa, $Y_c = -192$ MPa, $S = 62$ MPa. The strain limits of the corrugated

Table 3: Global strain limits for the example trapezoidal corrugation.

Strain Limit Item	Corrugated Panel	Flat Panel	Strain Limit Ratio (Corrugated/Flat)
Tension Strain $\bar{\epsilon}_x^t$	6.5954E-03	1.6667E-03	3.9572
Compression Strain $\bar{\epsilon}_x^c$	-6.2580E-03	-6.8571E-04	9.12631
Tension Strain $\bar{\epsilon}_y^t$	1.6667E-03	1.6667E-03	1
Compression Strain $\bar{\epsilon}_y^c$	-6.8571E-04	-6.8571E-04	1
Shear Strain $\lvert\bar{\gamma}_{xy}\rvert$	3.1385E-03	2.6000E-03	1.2071
Bending Strain $\lvert\bar{\kappa}_x\rvert$	8.2773E-01	6.8571E-01	1.2071
Bending Strain $\lvert\bar{\kappa}_y\rvert$	5.0052E-02	6.8571E-01	0.0730
Torsion Strain $\lvert\bar{\kappa}_{xy}\rvert$	2.6000E+00	2.6000E+00	1

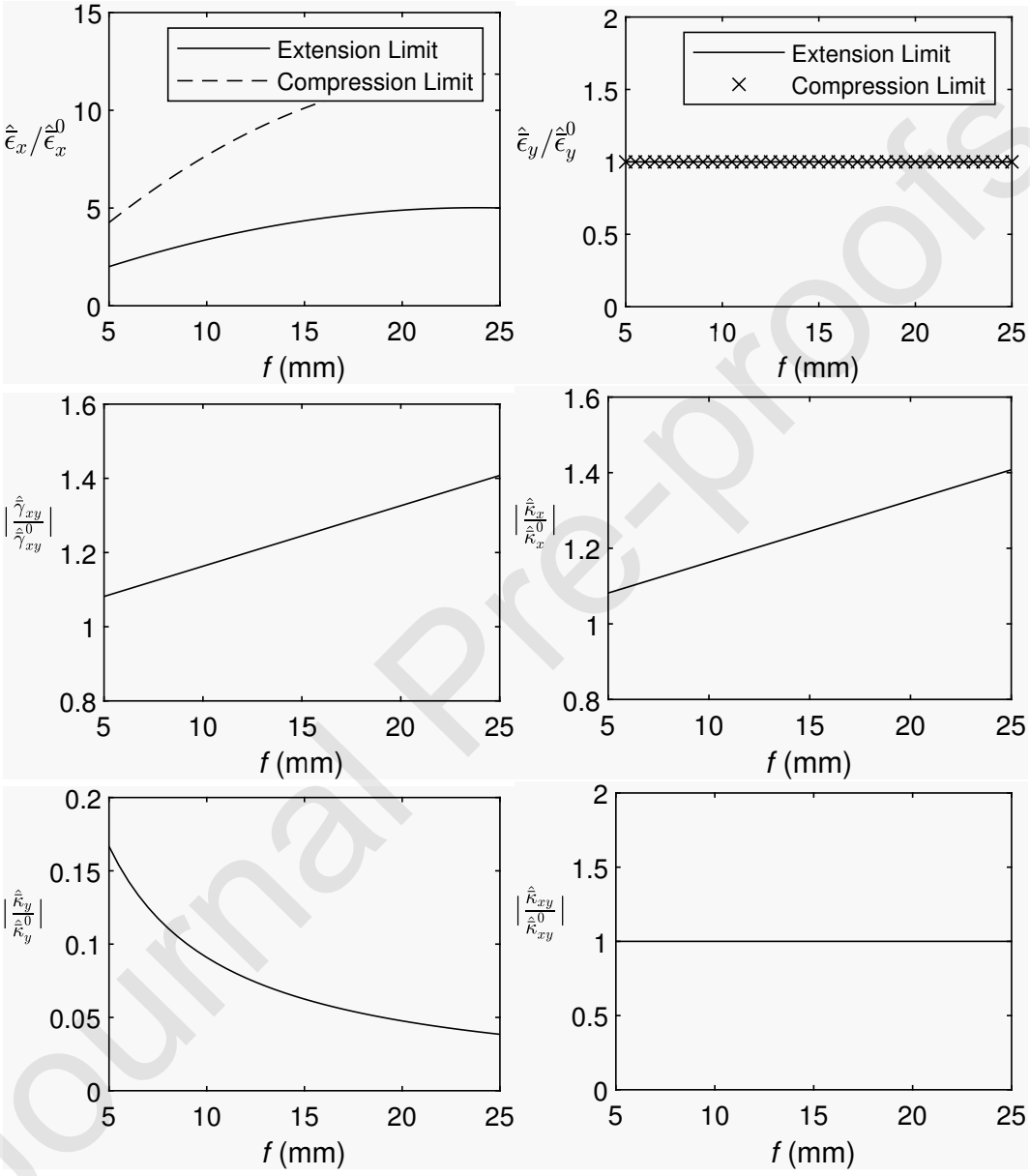

Figure 6: Normalised global strain limits with corrugation amplitude: trapezoidal corrugation

Table 4: Global strain limits for a single-layer round corrugated panel.

Strain Limit Item	Corrugated Panel	Flat Panel	Normalised strain limit (Corrugated/Flat)
Tension Strain $\bar{\epsilon}_x^t$	0.3093	0.0330	9.3825
Compression Strain $\bar{\epsilon}_x^c$	-0.2991	-0.0130	23.0761
Tension Strain $\bar{\epsilon}_y^t$	0.0048	0.0048	1
Compression Strain $\bar{\epsilon}_y^c$	-0.0142	-0.0142	1
Shear Strain $\lvert\bar{\gamma}_{xy}\rvert$	0.0357	0.0139	2.5683
Bending Strain $\lvert\bar{\kappa}_x\rvert$	111.0838	43.2098	2.5708
Bending Strain $\lvert\bar{\kappa}_y\rvert$	0.7643	16.0494	0.0476
Torsion Strain $\lvert\bar{\kappa}_{xy}\rvert$	46.3378	46.3378	1

Table 5: Global strain limits for a multiple-layer corrugated panel.

Strain Limit Item	Corrugated Panel	Flat Panel	Normalised Strain Limit (Corrugated/Flat)
Tension Strain $\bar{\epsilon}_x^t$	0.1072	0.0048	22.3333
Compression Strain $\bar{\epsilon}_x^c$	-0.1096	-0.0130	8.4308
Tension Strain $\bar{\epsilon}_y^t$	0.0048	0.0048	1
Compression Strain $\bar{\epsilon}_y^c$	-0.0130	-0.0130	1
Shear Strain $\lvert\bar{\gamma}_{xy}\rvert$	0.0247	0.0096	2.5729
Bending Strain $\lvert\bar{\kappa}_x\rvert$	39.6093	15.4074	2.5708
Bending Strain $\lvert\bar{\kappa}_y\rvert$	0.7955	41.4814	0.0192
Torsion Strain $\lvert\bar{\kappa}_{xy}\rvert$	44.4843	44.4843	1

panel and the flat panel are compared for both examples, which are shown in Tables 4 and 5 respectively.

The single-layer panel is further investigated to show the influence of the geometry parameters L, R and the thickness t. Figure 7 shows the variation of the normalised strain limit with the changing corrugation amplitude $f = R + L$ when the parameter $R = 3$mm and the thickness $t = 0.6$mm. Figure 8 shows the variation of the normalised strain limit with the corrugation shape proportionality factor k, defined such that all of the geometric parameters of the corrugation shape are multiplied by k. Hence the corrugation amplitude is $f = kR + kL$. The variation of the normalised strain limit is also shown in Figure 9 when the thickness of the panel changes.

5.3. Discussions

From Tables 3, 4 and 5, we can find that:

1) The axial strain limits of the corrugated panel in the x direction are amplified compared to flat panel. The amplification effect is due to the transformation coefficient T_{11} and T_{41}, which makes the maximum local strain along the s direction of the corrugated panel smaller than that in the flat panel.

2) The axial strain limits of the corrugated panel in the y direction are affected by the coefficients T_{22}, T_{12} and T_{42}. The local strains in the y direction is the same to those of the flat panel since the transformation coefficient $T_{22} = 1$; while the local strains in the s direction are functions of T_{12} and T_{42}. Both local strains in the y direction and in the s direction need to be within the strength limits. In the numerical examples above, both the tension and compression strain limits are identical to those of the flat panels since the local strains in the s direction are still within the strain limits while the local strain in the y direction reaches the failure point. It should be noted that for other cases, although the local strains in the y direction are always the same to those of the flat panel, the local strains in the s direction might reach an earlier failure than in the y direction.

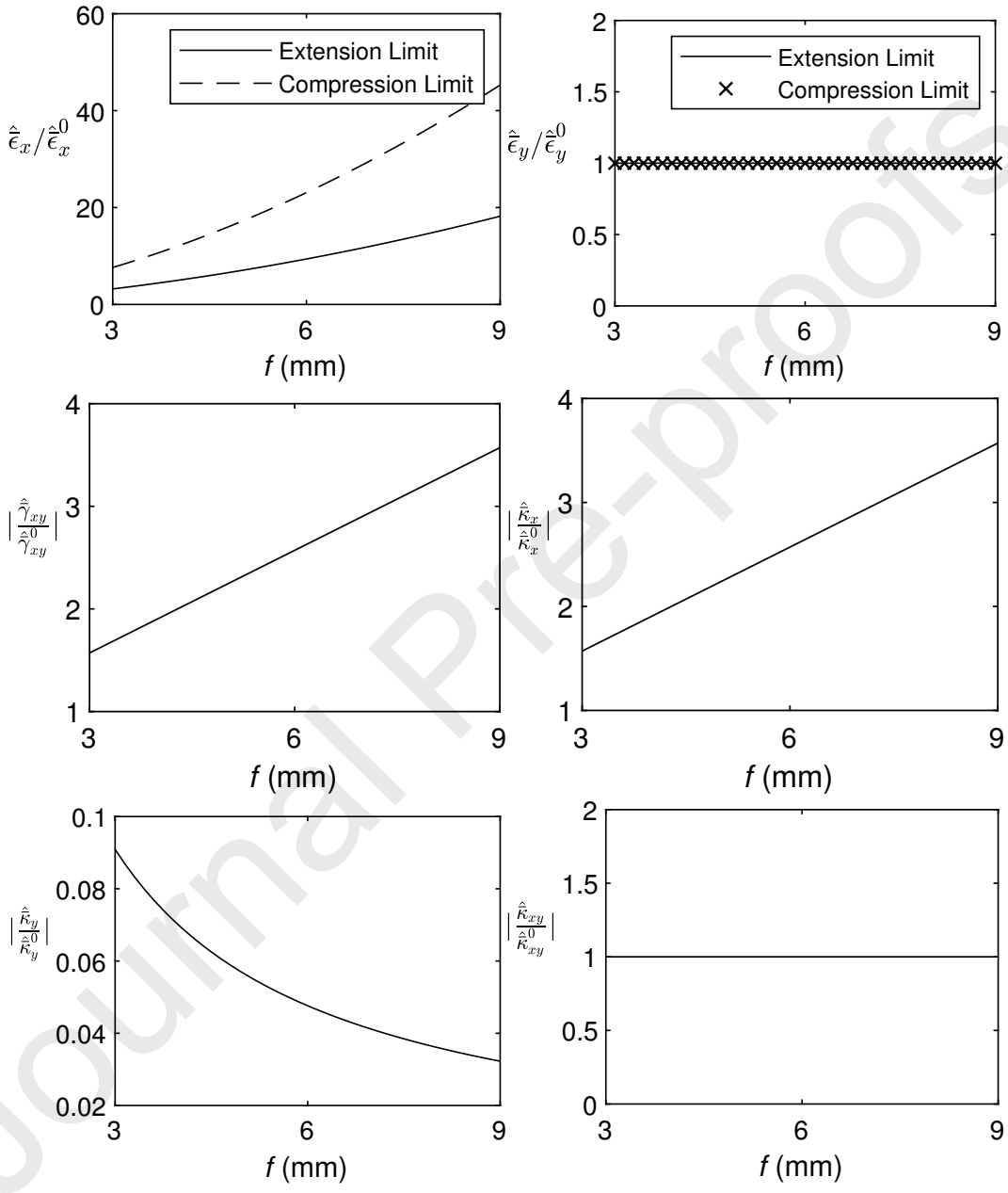

Figure 7: Normalised global strain limits with corrugation amplitude: round corrugation

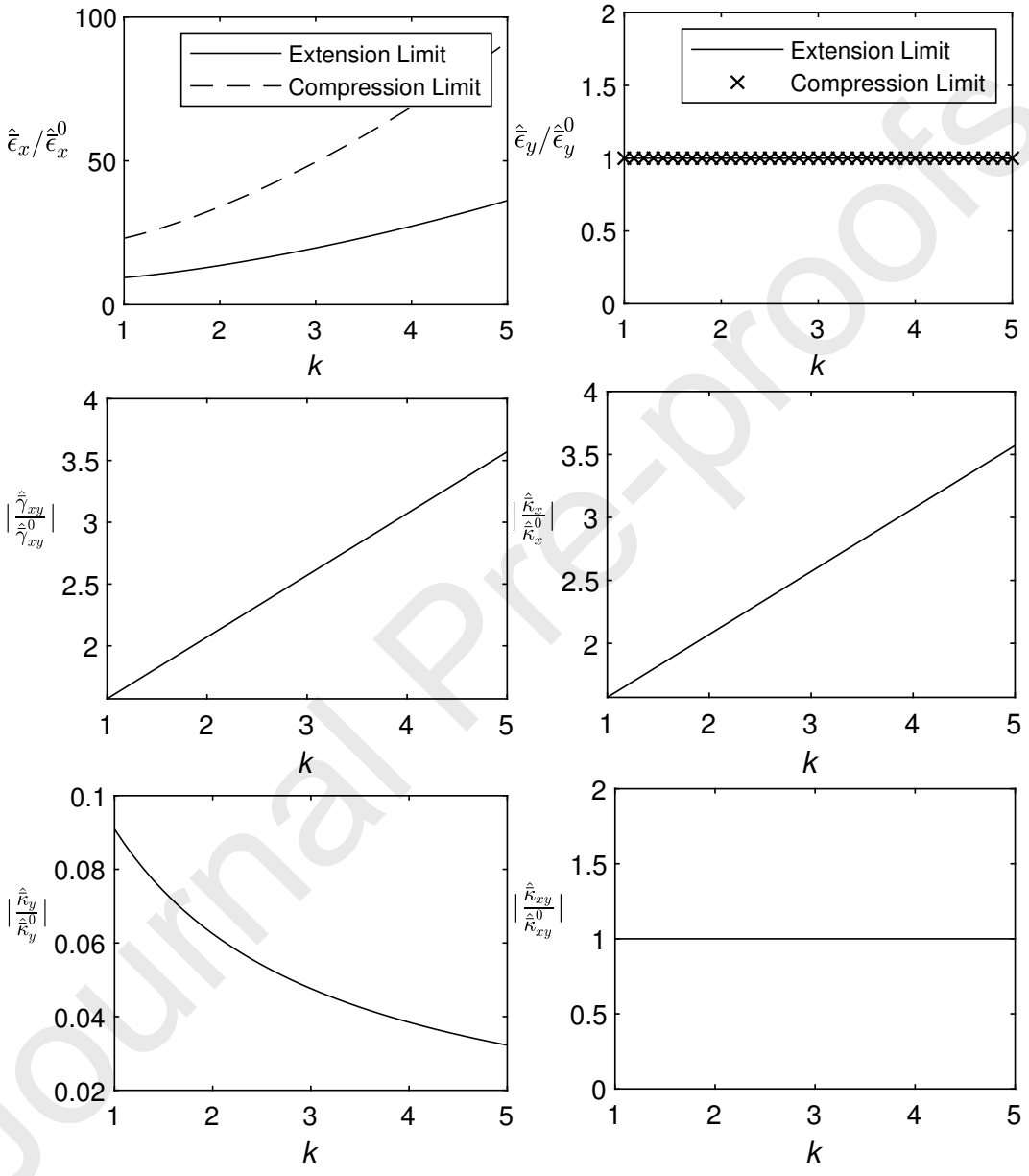

Figure 8: Normalised global strain limits with shape proportionality: round corrugation

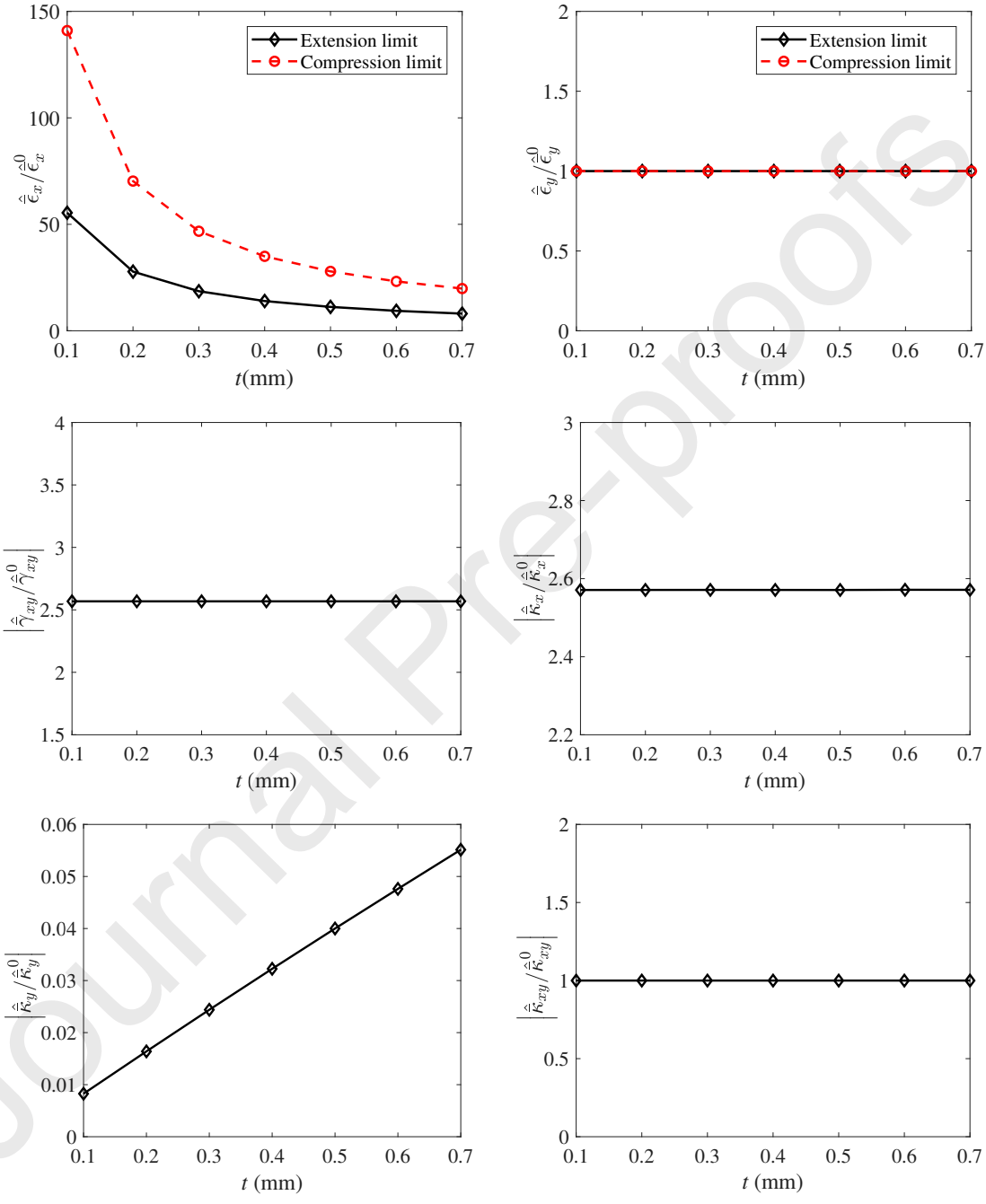

Figure 9: Normalised global strain limits with thickness: round corrugation

3) The shear strain limit of the corrugated panel is only affected by the transformation coefficient T_{33}, which is less than 1. As a result, the shear strain limit of the corrugated panel is larger than that of the flat panel.

4) The transformation coefficient T_{44} is smaller than 1, which means the local bending strain of the corrugated panel is less than that of the flat panel, hence the bending strain limit in the x direction of the corrugated panel is higher than the flat panel.

(5) The bending strain limit in the y direction of the corrugated panel is much lower than that of the flat panel. This is mainly because the local strain ϵ_y in the corrugated panel has an extra component $T_{25} * \bar{\kappa}_y$ compared to that of the flat panel, which is caused by bending in the y direction.

(6) The torsion strain is identical to that of the flat panel as the transformation coefficient $T_{66} = 1$.

It should also be noted that the local strain of a composite panel is determined by the composite stack sequence and the ply angles, when the middle strain and curvature components are obtained. In these case studies, the global bending strain $\bar{\kappa}_x$ reaches its limit when the local strain ϵ_1 exceeds the material strength in direction 1, while in the multi-layer panel, the local strain ϵ_2 exceeds the the material strength in direction 2 first.

Figures 6 and 7 shows the relationship between the normalised strain limit and the corrugation amplitude f. The normalised axial strain limit in the x direction, the shear strain limit and the bending strain limit in the x direction all increase with the corrugation amplitude f. While, the normalised bending strain limit in the y direction is always smaller than 1 and is reduced when f increases, which means that the corrugated panel has a very low capacity to withstand bending in the transverse direction. The normalised axial strain limit in the y direction and the torsion strain limits are the same as the strain limits of a flat panel and not affected by the amplitude f.

The results from the parametric analysis of the geometry parameter k for the round corrugation, presented in Figure 8, shows a similar trend. The

normalised axial strain limit in the x direction, the shear strain limit and the bending strain limit in the x direction all increase with the factor k. The normalised bending strain limit in the y direction decreases with the factor k. The axial strain limit in the y direction and the torsion strain limit are equal to 1 and not affected by the factor k.

The influence of the panel thickness is shown in Figure 9 for the round corrugated panel. The normalised axial strain limit in the x direction of the corrugated panel is reduced when the thickness increases. Although the normalised bending strain limit in the y direction increases with the panel thickness, the absolute limit of the corrugated panel is still smaller than that of the flat panel as the normalised limit is smaller than 1. The other normalised strain limits, i.e. the normalised axial strain limit in the y direction, the shear strain limit, the bending strain limit in the x direction and the torsion strain limit are not affected by the panel thickness. Although the absolute bending and torsion strain limits are reduced with the increase of the thickness, the corresponding strain limits of the flat panel are also reduced, which leads to the constant normalised strain limits.

6. Conclusion

In this paper, the relationship between the local and global strains of the corrugated panel is derived and the transformation matrix is built. Numerical simulation is used to validate the transformation matrix, which shows a good accuracy for both the trapezoidal and round corrugated panels. The mid-plane strain and curvature components can be obtained if the global strains of a corrugated panel are given. Then extreme values of the local strain can be further calculated from the mid-plane strains and curvatures using the classical plate theories, which makes it possible to predict the global strain limits of the corrugated panel. The maximum strain criterion is adopted in the current study, although other failure criterion could also be used if the index can be calculated from the mid-plane strains and curvatures. Case

studies are performed to show the influence of the corrugation geometry.

The derivation of the transformation matrix makes the quantitative investigation of the strain limits available. In addition to that, the following findings are listed from the perspective of applying corrugated panels in morphing aircraft,

1) Both the axial strain limit and the bending strain limit in the x direction of the corrugated panel are amplified by the corrugation geometry. And they can be further increased with the increasing corrugation amplitude f. This provides one of the reasons why the corrugated panel can be used as a candidate solution for morphing skins. The morphing structure should be deployed to allow the deformation to occur in the x direction of the corrugated panels, although increasing the thickness of the corrugated panel will reduce the strain limits in the x direction.

2) The axial strain limit of the corrugated panel in the y direction will not exceed the strain limit of the flat panel. The bending strain limit in the y direction is even smaller than that of the flat panel, which indicates that the capability of bending in transverse direction is weak. Therefore, large deformation should always be avoided in the y direction of the corrugated panel when it is used in a morphing structure.

3) The shear strain limit is amplified and can be increased with the corrugation amplitude, while the torsion limit remains the same as the flat panel and is not affected by the geometry parameters.

It should also be clarified that the current study is based on classical plate theory. If the original panel cannot be treated as a classical plate, then the transformation matrix will not be accurate enough. Also, the strain limit is predicated based on independent load cases. For practical applications, when multiple loadings are applied, linear superposition theory should be deployed.

7. References

[1] N. Buannic, P. Cartraud, T. Quesnel, Homogenization of corrugated core sandwich panels, Composite Structures 59 (3) (2003) 299–312.

[2] Z. Aboura, N. Talbi, S. Allaoui, M. L. Benzeggagh, Elastic behavior of corrugated cardboard: experiments and modeling, Composite Structures 63 (1) (2004) 53–62.

[3] R. Haj-Ali, J. Choi, B.-S. Wei, R. Popil, M. Schaepe, Refined nonlinear finite element models for corrugated fiberboards, Composite Structures 87 (4) (2009) 321–333.

[4] N. Talbi, A. Batti, R. Ayad, Y. Q. Guo, An analytical homogenization model for finite element modelling of corrugated cardboard, Composite Structures 88 (2) (2009) 280–289.

[5] J. Reany, J. L. Grenestedt, Corrugated skin in a foam core sandwich panel, Composite Structures 89 (3) (2009) 345–355.

[6] I. Dayyani, M. I. Friswell, S. Ziaei-Rad, E. S. Flores, Equivalent models of composite corrugated cores with elastomeric coatings for morphing structures, Composite Structures 104 (2009) 281–292.

[7] L. A. Carlsson, T. Nordstrand, B. Westerlind, On the elastic stiffnesses of corrugated core sandwich, Journal of Sandwich Sturctures and Materials 3 (2001) 253–267.

[8] Y. S. Tian, T. J. Lu, Optimal design of compression corrugated panels, Thin-Walled Structures 43 (3) (2005) 477–498.

[9] C. C. Liang, M. F. Yang, P. W. Wu, Optimum design of metallic corrugated core sandwich panels subjected to blast loads, Ocean Engineering 28 (7) (2001) 825–861.

[10] S. Barbarino, O. Bilgen, R. M. Ajaj, M. I. Friswell, D. J. Inman, A review of morphing aircraft, Journal of Intelligent Material Systems and Structures 22 (9) (2011) 823–877.

[11] S. Vasista, L. Tong, K. C. Wong, Realization of morphing wings: A multidisciplinary challenge, Journal of Aircraft 49 (1) (2012) 11–28.

[12] I. Dayyani, A. Shaw, E. S. Flores, M. Friswell, The mechanics of composite corrugated structures: A review with applications in morphing aircraft, Composite Structures 133 (2015) 358 – 380.

[13] D. Li, S. Zhao, A. D. Ronch, J. Xiang, J. Drofelnik, Y. Li, L. Zhang, Y. Wu, M. Kintscher, H. P. Monner, A. Rudenko, S. Guo, W. Yin, J. Kirn, S. Storm, R. D. Breuker, A review of modelling and analysis of morphing wings, Progress in Aerospace Sciences 100 (2018) 46 – 62.

[14] M. T. Kikuta, Mechanical properties of candidate materials for morphing wings, Master's thesis, Virginia Tech (2003).

[15] C. Thill, J. A. Etches, I. P. Bond, K. D. Potter, P. M. Weaver, Morphing skins - a review, The Aeronautical Journal 112 (2008) 117–139.

[16] T. Yokozeki, S.-I. Takeda, T. Ogasawara, T. Ishikawa, Mechanical properties of corrugated composites for candidate materials of flexible wing strucures, Composites Part A: Applied Science and Manufacturing 37 (2006) 1578–1586.

[17] C. Thill, J. A. Etches, I. P. Bond, K. D. Potter, P. M. Weaver, Composite corrugated structures for morphing wing skin applications, Smart Materials and Structures 19 (12) (2010) 124009.

[18] C. Thill, J. A. Etches, I. P. Bond, K. D. Potter, P. M. Weaver, M. R. Wisnom, Investigation of trapezoidal corrugated aramid/epoxy laminates under large tensile displacements transverse to the corrugation di-

rection, Composites Part A: Applied Science and Manufacturing 41 (1) (2010) 168–176, special Issue: Flow Processes in Composite Materials.

[19] D. Briassoulis, Equivalent orthotropic properties of corrugated sheets, Computers & Structures 23 (2) (1986) 129–138.

[20] D. E. McFarland, An investigation of the static stability of corrugated rectangular plates loaded in pure shear, Ph.D. thesis, University of Kansas (1967).

[21] A. Samanta, M. Mukhopadhyay, Finite element static and dynamic analysis of folded plates, Engineering Structures 21 (1999) 277–287.

[22] C. Thill, J. A. Etches, I. P. Bond, P. M. Weaver, K. D. Potter, Experimental and parametric analysis of corrugated composite structures for morphing skin applications, in: 19th International Conference on Adaptive Structures and Technologies, Ascona, Switzerland, 2008.

[23] G. Kress, M. Winkler, Corrugated laminate homogenization model, Composite Structures 92 (2010) 795–810.

[24] G. Kress, M. Winkler, Corrugated laminate analysis: A generalized plane-strain problem, Composite Structures 93 (5) (2011) 1493–1504.

[25] D. Filipovic, G. Kress, A planar finite element formulation for corrugated laminates under transverse shear loading, Composite Structures 201 (2018) 958 – 967.

[26] D. Filipovic, G. Kress, Stress analysis of corrugated orthotropic laminates under transverse shear loading, Composite Structures 223 (2019) 110983. doi:https://doi.org/10.1016/j.compstruct.2019.110983.

[27] I. Dayyani, S. Ziaei-Rad, H. Salehi, Numerical and experimental investigations on mechanical behavior of composite corrugated core, Applied Composite Materials 19 (3) (2012) 705–721.

[28] G. Bartolozzi, M. Pierin, U. Orrenius, N. Baldanzini, An equivalent material formulation for sinusoidal corrugated cores of structural sandwich panels, Composite Structures 100 (2013) 173–185.

[29] Z. Ye, V. L. Berdichevsky, W. Yu, An equivalent classical plate model of corrugated structures, International Journal of Solids and Structures 51 (11) (2014) 2073 – 2083.

[30] H. Mohammadi, S. Ziaei-Rad, I. Dayyani, An equivalent model for trapezoidal corrugated cores based on homogenization method, Composite Structures 131 (2015) 160 – 170.

[31] C. Wang, H. H. Khodaparast, M. I. Friswell, A. D. Shaw, An equivalent model of corrugated panels with axial and bending coupling, Computers Structures 183 (2017) 61 – 72.

[32] J.-B. Bai, D. Chen, J.-J. Xiong, C.-H. Dong, A semi-analytical model for predicting nonlinear tensile behaviour of corrugated flexible composite skin, Composites Part B: Engineering 168 (2019) 312 – 319.

[33] G. Kress, D. Filipovic, An analytical nonlinear morphing model for corrugated laminates, Curved and Layered Structures 6 (1) (2019) 57–67.

[34] D. Filipovic, G. Kress, Manufacturing method for high-amplitude corrugated thin-walled laminates, Composite Structures 222 (2019) 110925. doi:https://doi.org/10.1016/j.compstruct.2019.110925.

[35] M. Winkler, G. Kress, Deformation limits for corrugated cross-ply laminates, Composite Structures 92 (6) (2010) 1458–1468.

[36] A. Schmitz, P. Horst, Bending deformation limits of corrugated unidirectionally reinforced composites, Composite Structures 107 (2014) 103 – 111.

[37] Y. Xia, M. I. Friswell, E. I. Saavedra Flores, Equivalent models of corrugated panels, International Journal of Solids and Structures 49 (13) (2012) 1453–1462.

[38] Dassault Systemes SE, Abaqus 2016 Document: Abaqus Analysis User's Guide, 2016.

[39] S. R. Soni, A comparative study of failure envelopes in composite laminates, Journal of Reinforced Plastics and Composites 2 (1983) 34–42.